Design of Robust Distributed Control for Interconnected Microgrids

M. J. Hossain, *Senior Member, IEEE*, M. A. Mahmud, *Member, IEEE*, F. Milano, *Senior Member, IEEE*, S. Bacha, *Member, IEEE*, A. Hably, *Member, IEEE*

Abstract—This paper proposes a distributed control scheme to regulate the power flows among multiple microgrids operating in islanded mode. Each microgrid controller gathers information from neighboring microgrids and reduces dynamic interactions. Modal analysis and time-domain simulations are used to identify critical issues that degrade the stability of microgrids under different operating conditions. A case study comprising three interconnected microgrids is considered. Each microgrid includes distributed generation and is described through a detailed dynamic model. Time-domain analyses are carried out considering different scenarios and large disturbances. Simulation results indicate that, while conventional controllers can lead to poorly damped power oscillations among the interconnected microgrids, the proposed control scheme guarantees stability in the post-disturbance operating conditions.

Keywords—*Microgrid, oscillation damping, distributed control, decentralized control, robust control.*

I. Introduction

MICROGRIDS are currently controlled independently, according to local requirements and aims, often based on local control strategies and without coordination with other microgrids [1], [2]. However, it is anticipated that future sub-transmission and distribution systems will be composed of several interconnected microgrids and form a complex electric network. Interconnecting together multiple microgrids can lead to undesirable dynamic behaviors, which have not been adequately examined so far. In particular, this paper discusses power oscillations arising from multiple interconnected microgrids and proposes a control scheme based on a robust distributed control approach.

A. Literature Review

1) Benefits of microgrid interconnection: A single microgrid system can only generate and distribute power within a localized area. In addition, the intermittent power generated by solar photovoltaic (PV) units and wind turbines often cause variations in the output power, voltage and frequency. Furthermore, in the event of unavailability/failure of one or more distributed

M. J. Hossain is with Griffith School of Engineering, Griffith University, Gold Coast, QLD-4215, Australia. Email: j.hossain@griffith.edu.au

M. A. Mahmud is with School of Engineering, Deakin University, Geelong, VIC 3216. Email: apel.mmahmud@deakin.edu.au

F. Milano is with Electricity Research Centre, EECE, University College Dublin, Dublin, Ireland. Email: federico.milano@ucd.ie

S. Bacha and A. Hably are with the G2ELab and Gipsa-lab, respectively, Joseph Fourier University of Grenoble, France. Email: seddik.bacha@g2elab.grenoble-inp.fr

generation (DG) units in the single microgrid system during the islanded mode of operation, the single microgrid system itself will not be secured enough to meet its own load demand due to restricted energy generation capability. In such cases, the single microgrid system usually employs load shedding technique to ensure supply-demand balance which is usually inconvenient and economically undesirable as it poses the risk of causing disruption to customers' business operations. In order to overcome the above mentioned challenge in a single microgrid system, the interconnection of microgrids is proposed in this paper as multiple microgrid systems in adjacent locations can be interconnected to exchange power with each other in order to ensure the improved security of supply.

The feasibility and benefits of interconnecting microgrids have been discussed in the literature. An electricity cluster oriented network is proposed in [3] where an inverter is used to connect the clusters. In [3], the authors propose a grid-independent power network that comprises of one or several clusters in which DG units and energy storage systems (ESSs) are the main power supply sources. In [4], it is shown that several smart grid functions, for example, improved reliability, high penetrations of renewable energy and improved generation efficiency can be achieved using coupled microgrids. An agent-based intelligent power management system is proposed in [5] to facilitate power trading among microgrids. The references above discuss the benefits of coupled microgrids. The focus of this paper is investigating dynamic interactions of multiple microgrids and their impacts on the dynamic performance of distribution systems. Another aim of this paper is to design a robust controller to minimize the unwanted negative interactions of multiple microgrids.

2) Control of islanded microgrids: The control of islanded microgrids with non/less inertial DG units is a great challenge for future power industries. Without a reliable and robust control strategy, serious issues (e.g., voltage profile degradation, frequency instability and loss of synchronization) can occur in the system. Clustered and agent-based controls are proposed in [6]–[8] for controlling multiple microgrids. A cooperative control approach for voltage control based on reactive power sharing among groups of DG units is proposed in [9]. A technique to model and stabilize a large microgrid for small-signal analysis is discussed in [10], whereas a three-level hierarchical control is proposed in [11]. In [12], the authors suggest an optimal reactive power control strategy which is based on a centralized architecture that requires expensive and reliable communication systems. Recently, decentralized volt-

age control schemes to minimize distribution power losses of microgrids have been proposed in [13]–[15]. These references use proportional-integral (PI) controllers to design voltage and power controllers that work well for a particular operating condition. The authors in [16], [17] propose decentralized droop controllers for islanded microgirds. The controllers discussed above cannot ensure the stable operation during large disturbances, e.g., islanding from grid-connected mode, as these are not designed considering the information from neighboring microgrids.

3) Distributed control of microgrids: Distributed control is becoming more and more popular to control clustered microgrids with DG units and ESSs as it is significantly difficult to manage and control a large number of DG units using either centralized or decentralized control. Distributed control uses local communication networks and includes the positive features of both centralized or decentralized controls while reducing the effects of their drawbacks [18]. A self-organizing distributed power flow control for simplified models of PV units connected to distribution systems is proposed in [19]. In [20], the authors propose a distributed control for power sharing and voltage control in DC microgrids. A model predictive distributed control is proposed in [21] to maintain the voltage profile of a multi-area power system within the acceptable bounds. The nonlinearities and dynamics of the system are neglected in [20], [21]. A distributed hierarchical control architecture for automatic generation control is proposed in [22] for large-scale power systems by considering the dynamics of synchronous generators but this is not the case of interconnected microgrids in islanded operational mode.

4) Interconnection of microgrids: The management of power flows is a challenge in interconnected microgrids. A custom interconnection architecture for multiple microgrids is proposed in [23], whereas, in [24], the authors present a multi-agent based decentralized control scheme for power management in microgrids. A load management scheme in interconnected microgrides to reduce the operational cost is proposed in [25]. However, in the above mentioned literature, nonlinear dynamical models are not considered to design the controllers of DG units. A distributed control scheme is presented in [26] to regulate power flows among multiple microgrids. In [27], the authors present a model predictive control scheme for optimal power exchanges in a smart network of microgrids. System uncertainties, which are essential for the design of robust controllers, are neglected in [26], [27].

B. Contribution

This paper investigates the dynamic interactions among interconnected microgrids. To allow the islanded operation mode, each microgrid includes DG units (a PV and full converter-based wind generator (WG) system) and a STAT-COM/ESS. The paper shows that the interaction of standard microgrid controllers can lead to poorly damped oscillations. These oscillations can be effectively damped through a proper regulation of ESS active powers as well as STATCOM reactive powers. The main contribution of this paper is the development of a robust distributed control scheme to achieve the

desired power regulation by coordinating DG units and STAT-COM/ESSs of each microgrid. The design process considers the uncertainties and system nonlinearities which enhances the robustness of the closed-loop system. It monitors the power mismatch in neighbouring microgrids and regulates power flow among different microgrids. The proposed control scheme is robust, insensitive to parametric uncertainties and can cope with system nonlinearities.

C. Paper organization

The remainder of the paper is organized as follows. Section II provides the mathematical modeling of an inverter-based microgrid. The general formulation of the system model and incorporation of uncertainties within the model are also presented in Section II. The proposed control strategy and design algorithm are discussed in Section III. In Section IV, a case study composed of three interconnected microgrids is used for illustrating negative interactions and discussing the performance of the distributed controller. Finally, concluding remarks are presented in Section V.

II. MICROGRID MODEL

An accurate nonlinear dynamical model of a microgrid is crucial for stability analysis and controller design. The remainder of this section is organized as follows. Nonlinear models of each element of the microgrid, namely, distributed generators, loads, lines, STATCOM and ESS devices, are described in details. Distributed generators, loads and lines are modeled in a single block, hereinafter called a *subsystem*. Then, a general compact notation is proposed where linear terms are separated from nonlinear ones. Parameter uncertainties are also modeled to ensure the robustness of the design of the proposed control scheme.

A. Subsystem model

Each microgrid subsystem is assumed composed of a DG with a series RL branch, a load and a line, as depicted in Fig. 1.
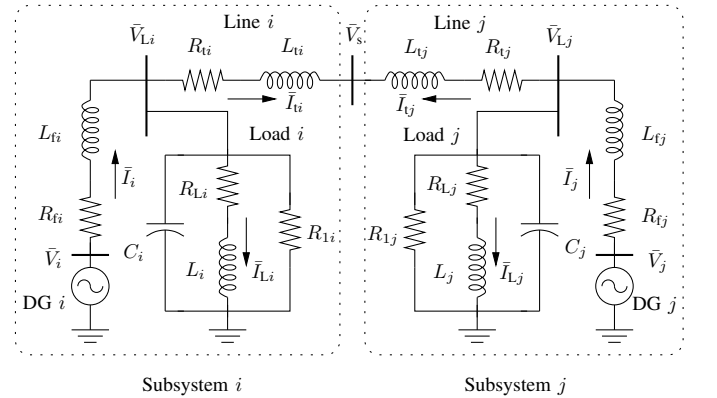

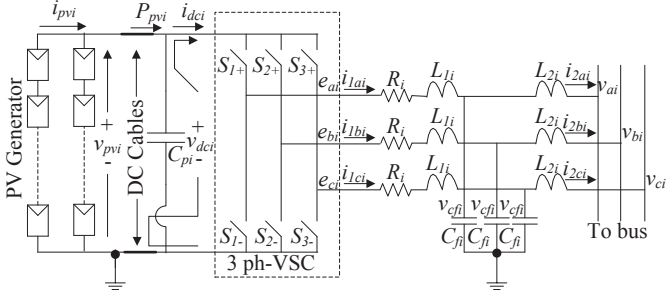Fig. 1.   Single line diagram of two subsystems that compose a microgrid.

Fig. 2. PV system connected to the grid.

The DG voltage source is controlled through a voltage source converter (VSC) device, hence $\bar{V}_i = k_i m_i V_{ci} \angle \alpha_i$, where V_{ci} is the DC voltage source equivalent to the DG unit, α_i is the VSC firing angle, k_i is the converter ratio and m_i is the VSC modulation index. The series RL branch includes R_{fi}, which is the equivalent resistance accounting for the switching and transformer losses; and L_{fi}, which is the leakage reactance of the transformer. Loads are represented as parallel RLC branches (R_{1i}, R_{Li}, C_i, L_i) and lines are represented as series RL branches where R_{ti} and L_{ti} are distribution line resistance and inductance, respectively. According to Fig. 1 and the description above, the full model of the i-th subsystem in dq frame is given by [28]:

$$L_{fi}\dot{I}_{di} = V_{di} - R_{fi}I_{qi} + \omega_i I_{qi}L_{fi} - V_{Ldi} \qquad (1)$$
$$L_{fi}\dot{I}_{qi} = V_{qi} - R_{fi}I_{di} - \omega_i I_{di}L_{fi} - V_{Lqi}$$
$$L_{ti}\dot{I}_{tdi} = V_{Ldi} - R_{ti}I_{tqi} + \omega_i I_{tqi}L_{ti} - V_{sd}$$
$$L_{ti}\dot{I}_{tqi} = V_{Lqi} - R_{ti}I_{tdi} - \omega_i I_{tdi}L_{ti} - V_{sq}$$
$$L_i\dot{I}_{Ldi} = V_{Ldi} - R_{Li}I_{Lqi} + \omega_i I_{Lqi}L_i$$
$$L_i\dot{I}_{Lqi} = V_{Lqi} - R_{Li}I_{Ldi} - \omega_i I_{Ldi}L_i$$
$$C_i\dot{V}_{Ldi} = I_{di} - I_{tdi} + \omega_i V_{Lqi}C_i - I_{Ldi} - (1/R_{1i})V_{Lqi}$$
$$C_i\dot{V}_{Lqi} = I_{qi} - I_{tqi} - \omega_i V_{Ldi}C_i - I_{Lqi} - (1/R_{1i})V_{Ldi}$$

where I_{Ldi} and I_{Lqi} are the dq components of the current through the load; I_{di} and I_{qi} are the dq components of the DG unit's current; I_{tdi} and I_{tqi} are the dq components of the current through the line; $\omega_i = 2\pi f_i$ is the subsystem angular speed and $V_{Li} = \sqrt{V_{Ldi}^2 + V_{Lqi}^2}$ is the load voltage. Observe that the nonlinearity of (1) is basically due to the dependence on the subsystem frequency f_i that, in islanded mode, is determined by the active power droop control. Observe also that subsystems are connected at a point of connection, whose voltage is $\bar{V}_s$ in Fig. 1. Finally, the active and reactive powers injected by the DG units at the i-th bus are:

$$P_i = \frac{3}{2}\left(V_{Lqi}I_{qi} + V_{Ldi}I_{di}\right) \qquad (2)$$
$$Q_i = \frac{3}{2}\left(V_{Lqi}I_{di} - V_{Ldi}I_{qi}\right)$$
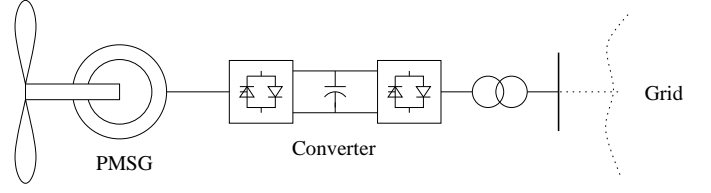

Fig. 3. Schematic diagram of PMSG-based wind turbine.

B. DG units

In this paper, photovoltaic (PV) units and permanent magnet synchronous generators (PMSG)-based wind generator are considered as DG units and their output voltages are $\bar{V}_i$ as shown in Fig. 1. The PV system consists of PV panels, a three-phase VSC and an output LCL filter. The nonlinear model of a three phase grid-connected PV system can be obtained from Fig. 2 in dq frame using the angular frequency ω of the grid and is given as [29]:

$$L_{1i}\dot{I}_{1di} = -R_i I_{1di} - \omega_i L_{1i}I_{1qi} + R_i I_{2di} - V_{cfdi} + v_{pv}K_{di} \qquad (3)$$
$$L_{1i}\dot{I}_{1qi} = -R_i I_{1qi} + \omega_i L_{1i}I_{1di} + I_{2qi} - V_{cfqi} + V_{pv}K_{qi}$$
$$L_{2i}\dot{I}_{2di} = R_i I_{1di} - R_i I_{2di} - \omega_i L_{2i}I_{2qi} + V_{cfdi} - V_{di}$$
$$L_{2i}\dot{i}_{2qi} = R_i I_{1qi} - R_i I_{2qi} + \omega_i L_{2i}I_{2di} + V_{cfqi} - V_{qi}$$
$$C_{fi}\dot{V}_{cfdi} = -\omega_i C_{fi}V_{cfqi} + C_{fi}\left(I_{1di} - I_{2di}\right)$$
$$C_{fi}\dot{V}_{cfqi} = \omega_i C_{fi}V_{cfdi} + C_{fi}\left(I_{1qi} - I_{2qi}\right)$$
$$C_{pi}\dot{V}_{pvi} = I_{pvi} - I_{1di}K_{di} - I_{1qi}K_{qi}$$

where R_i is the resistance, L_{1i} and L_{2i} are the inductances of the filter, C_{pi} is the DC capacitance, C_{fi} is the filter capacitance, V_{pvi} is the voltage across the DC-link capacitor, V_{cf} is the voltage across the filter capacitor, I_{1i} and I_{2i} are the output currents of the inverter and filter, respectively, ω_i is the angular frequency, I_{pvi} is the output current of PV array, K_{di} and K_{qi} are the binary input switching signals, respectively. The subscripts d_i and q_i stand for direct and quadrature component, and f_i for filter.

The PMSG is used in the variable-speed wind generation systems. Figure 3 shows the schematic diagram of a wind turbine with PMSG connected to the point of common coupling (PCC) through a transformer. The nonlinear model of the wind turbine, made up of the various blocks shown in Fig. 3, is based on a static model of the aerodynamics, a nonlinear model of the generator, the network-side-converter (NSC) with DC-link capacitor, grid-side filter and the generator-side-converter (GSC). The aerodynamic torque applied to the rotor of the turbine by the effective wind speed passing through the rotor is given as [29]:

$$T_{aei} = \frac{\rho_i}{2\omega_{mi}} A_{wti}c_{pi}(\lambda_i, \theta_i)V_{wi}^3 \qquad (4)$$

where the symbols follow the notation as discussed in [29]. When the direction of d-axis is aligned with rotors magnetic flux linkage, the transient model of a PMSG is described in
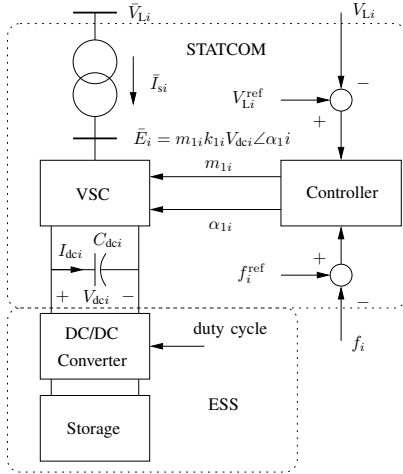
Fig. 4. STATCOM/ESS control scheme.

this paper by the following equations [30]:

$$V_{\mathrm{ds}i} = R_{\mathrm{w}i}I_{\mathrm{dws}i} - \omega_{\mathrm{s}i}\psi_{\mathrm{qs}i} + \dot{\psi}_{\mathrm{ds}i} \tag{5}$$
$$V_{\mathrm{qs}i} = R_{\mathrm{w}i}I_{\mathrm{qws}i} + \omega_{\mathrm{s}i}\psi_{\mathrm{qs}i} + \dot{\psi}_{\mathrm{qs}i}$$

where V_i is the voltage, I_i is the current, $R_{\mathrm{w}i}$ is the resistance and ψ_i is the flux. The subscripts d_i and q_i stands for direct- and quadrature-axis components, and w_i for wind turbine.

The dynamics of the the GSC can be written as [30]:

$$L_{\mathrm{dws}i}\dot{I}_{\mathrm{dws}i} = -R_{\mathrm{ws}i}I_{\mathrm{dws}i} - \omega_{\mathrm{s}i}I_{\mathrm{gws}i}L_{\mathrm{qw}i} - V_{\mathrm{ds}i} \tag{6}$$
$$L_{\mathrm{qw}i}\dot{I}_{\mathrm{qws}i} = -R_{\mathrm{ws}i}I_{\mathrm{qws}i} + \omega_{\mathrm{s}i}I_{\mathrm{dws}i}L_{\mathrm{dw}i} - V_{\mathrm{qs}i}$$

The dynamics of the the NSC is given as [30]:

$$L_{\mathrm{f}i}\dot{I}_{\mathrm{dwn}i} = -R_{\mathrm{wf}i}I_{\mathrm{dwn}i} - \omega_{\mathrm{s}i}I_{\mathrm{gwn}i}L_{\mathrm{w}i} - V_{\mathrm{ds}i} + V_{\mathrm{d}i} \tag{7}$$
$$L_{\mathrm{w}i}\dot{I}_{\mathrm{qwn}i} = -R_{\mathrm{wf}i}I_{\mathrm{qwn}i} + \omega_{\mathrm{s}i}I_{\mathrm{dwn}i}L_{\mathrm{f}i} - V_{\mathrm{qs}i} + V_{\mathrm{q}i}$$

The DC-link dynamics are represented as:

$$C_{\mathrm{wdc}i}V_{\mathrm{wdc}i}\dot{V}_{\mathrm{wdc}i} = -\frac{V_{\mathrm{dc}i}^2}{R_{\mathrm{loss}i}} - P_{\mathrm{t}i} - P_{\mathrm{n}i}, \tag{8}$$

where resistor $R_{\mathrm{loss}i}$ represents the total conducting and switching losses of the GSC and $C_{\mathrm{dc}i}$ is the capacitance. Also, $P_{\mathrm{n}i}$ is the wind generator output power, and $P_{\mathrm{w}i}$ is the power delivered to the network.

C. STATCOM and ESS model

Fast and independent active and reactive power support provided by a STATCOM/ESS can significantly enhance the performance of microgrids. Hence, STATCOM/ESS devices are included in the microgrid model in parallel to a load as shown in Fig. 4.

The voltage across the i-th STATCOM/ESS is V_{L_i}. A standard STATCOM device is comprised of a coupling transformer, a VSC, and a DC-link capacitor (see $C_{\mathrm{dc}i}$ in Fig. 4). The DC-link capacitor provides voltage supports for the VSC and the DC chopper. The ESS consists of a storage device (e.g., a bank

of batteries) and a bi-directional DC-DC buck-boost converter to control the charging and discharging of the storage device. The aim of ESS modules is to store and/or deliver energy to the grid via the DC-link whenever required. The VSC model is given as in [31]:

$$L_{\mathrm{s}i}\dot{I}_{\mathrm{ds}i} = -R_{\mathrm{s}i}I_{\mathrm{ds}i} + L_{\mathrm{s}i}I_{\mathrm{qs}i}\omega_i + V_{\mathrm{Ld}i} - E_{\mathrm{d}i}$$
$$L_{\mathrm{s}i}\dot{I}_{\mathrm{qs}i} = -R_{\mathrm{s}i}I_{\mathrm{qs}i} - L_{\mathrm{s}i}I_{\mathrm{ds}i}\omega_i + V_{\mathrm{Lq}i} - E_{\mathrm{q}i} \tag{9}$$
$$\dot{V}_{\mathrm{dc}i} = -\frac{1}{C_{\mathrm{dc}i}}I_{\mathrm{dc}i} = -\frac{1}{C_{\mathrm{dc}i}}(I_{\mathrm{dc}1i} - I_{\mathrm{dc}2i})$$

where $E_{\mathrm{d}i} = k_{1i}m_{1i}V_{\mathrm{dc}i}\cos\alpha_{1i}$, $E_{\mathrm{q}i} = k_{1i}m_{1i}V_{\mathrm{dc}i}\sin\alpha_{1i}$ and $I_{\mathrm{dc}1i}$ and $I_{\mathrm{dc}1i}$ are given by

$$I_{\mathrm{dc}1i} = \frac{V_{\mathrm{dc}i} - E_{\mathrm{b}i}}{R_{\mathrm{b}i}}m_{2i}k_{2i}(\cos\alpha_{2i} + \sin\alpha_{2i})$$
$$I_{\mathrm{dc}2i} = m_{1i}k_{1i}I_{\mathrm{ds}i}\cos\alpha_{1i} + m_{1i}k_{1i}I_{\mathrm{qs}i}\sin\alpha_{1i} \tag{10}$$

$V_{\mathrm{dc}i}$ is the capacitor voltage, $C_{\mathrm{dc}i}$ is the DC capacitor, $R_{\mathrm{dc}i}$ is the internal resistance of the capacitor, and $P_{\mathrm{s}i}$ is the power supplied by the system to the STATCOM to charge the capacitor. The STATCOM terminal AC voltage is $\bar{E}_i = k_{1i}V_{\mathrm{dc}i}\angle\alpha_{1i}$, where k_{1i} is the inverter ratio, m_{1i} and α_{1i} are the modulation ratio and phase angle of VSC of the STATCOM. The ESS is modeled as a battery ($E_{\mathrm{b}i}$) and the converter switching losses are represented by a resistance $R_{\mathrm{b}i}$ in parallel with a battery. Finally, m_{2i} and α_{2i} are the modulation ratio and phase angle of the DC-DC converter.

D. General formulation and inclusion of nonlinearity and uncertainty

Conventional control design methods are based on linear models that provide adequate performance in the neighborhood of a given operating condition. However, microgrids can show large variations of generation and loading levels. In this paper, nonlinearity is preserved and such variations are taken into account through a parameteric analysis of uncertainties.

The models described by (1)-(10) can be represented in a compact form as:

$$\dot{\boldsymbol{x}}_i = \boldsymbol{A}_i\boldsymbol{x}_i + \boldsymbol{B}_i[\boldsymbol{u}_i + \boldsymbol{\psi}_i(\boldsymbol{x}_i)]$$
$$\boldsymbol{y}_i = \boldsymbol{C}_i\boldsymbol{x}_i \tag{11}$$

where

$$\boldsymbol{x}_i = [I_{\mathrm{d}i}, I_{\mathrm{q}i}, I_{\mathrm{td}i}, I_{\mathrm{tq}i}, V_{\mathrm{Ld}i}, V_{\mathrm{Lq}i}, I_{\mathrm{Ld}i}, I_{\mathrm{Lq}i},$$
$$I_{1\mathrm{d}i}, I_{1\mathrm{q}i}, I_{2\mathrm{d}i}, I_{2\mathrm{q}i}, V_{\mathrm{cfd}i}, V_{\mathrm{cfq}i}, V_{\mathrm{pv}i}, \psi_{\mathrm{ds}i},$$
$$\psi_{\mathrm{qs}i}, I_{\mathrm{dws}i}, I_{\mathrm{qws}i}, I_{\mathrm{dwn}i}, I_{\mathrm{qwn}i}, V_{\mathrm{wdc}i}, I_{\mathrm{ds}i}, I_{\mathrm{qs}i}, V_{\mathrm{dc}i}]^T$$

is the state vector of the i-th agent. For STATCOM VSC control $\boldsymbol{u}_i = [m_{1i}, \alpha_{1i}]^T$ is the control input and $\boldsymbol{y}_i = [V_{L_i}, f_i]^T$ is the measured output. For inverter, $\boldsymbol{u}_i = [m_i, \alpha_i]^T$ and $\boldsymbol{y}_i = [P_i, Q_i, f_i]^T$ and for DC-DC converter, $\boldsymbol{u}_i = [m_{2i}, \alpha_{2i}]^T$ and $\boldsymbol{y}_i = [V_{DCi}, E_{bi}]^T$. The matrices $\boldsymbol{A}_i$, $\boldsymbol{B}_i$ and $\boldsymbol{C}_i$ are constant and known, and describe nominal subsystem model. The uncertainty $\boldsymbol{\psi}_i(\boldsymbol{x}_i)$ represent unmodeled parts of nonlinear terms, and disturbances due to unmodeled parts which are

calculated from the higher-order terms, known as the Cauchy remainder, in the Taylor series [33]:

$$(\boldsymbol{M}_i - \boldsymbol{A}_i)\Delta\boldsymbol{x}_i = \boldsymbol{\psi}_i(\boldsymbol{x}_i) = \boldsymbol{W}_i^T\boldsymbol{\varphi}_i(\boldsymbol{x}_i) + \boldsymbol{\epsilon}_i, \qquad (12)$$

where

$$\boldsymbol{M}_i = \left[\left.\frac{\partial\boldsymbol{f}_{i1}}{\partial\boldsymbol{x}_i}\right|_{\substack{x_i=x_i^{*1}\\u_i=u_i^{*1}}}, \ldots, \left.\frac{\partial\boldsymbol{f}_{i25}}{\partial\boldsymbol{x}_i}\right|_{\substack{x_i=x_i^{*N}\\u_i=u_i^{*N}}} \right]^T,$$

where $\boldsymbol{x}_i$ is a 1×25 column vector, $fi = [f_{i1}, \ldots, f_{i25}]^T$ is also a 1×25 column vector made up of the right-hand sides of (1)-(10), (x_i^{*N}, u_i^{*N}), $N = 1, \ldots, 25$, denote points lying on the line segment connecting points (x_i, u_i) and (x_{i_0}, u_{i_0}) and the constant matrix $\boldsymbol{W}_i$ is [33]:

$$\boldsymbol{W}_i = \mathrm{diag}\left[\frac{R_{\mathrm{f}i}}{L_{\mathrm{f}i}}, \frac{R_{\mathrm{f}i}}{L_{\mathrm{f}i}}, \frac{R_{\mathrm{t}i}}{L_{\mathrm{t}i}}, \frac{R_{\mathrm{t}i}}{L_{\mathrm{t}i}}, \frac{1}{R_{\mathrm{L}i}C_i}, \frac{1}{R_{\mathrm{L}i}C_i}, \right. \qquad (13)$$
$$\frac{R_{\mathrm{L}i}}{L_i}, \frac{R_{\mathrm{L}i}}{L_i}, \frac{R_i}{L_{1i}}, \frac{R_i}{L_{1i}}, \frac{R_i}{L_{2i}}, \frac{R_i}{L_{2i}}, 0, 0, 0, 0, 0, \frac{R_{\mathrm{ws}i}}{L_{dwi}},$$
$$\left.\frac{R_{\mathrm{ws}i}}{L_{qwi}}, \frac{R_{\mathrm{wf}i}}{L_{wfi}}, \frac{R_{\mathrm{wf}i}}{L_{wfi}}, \frac{1}{C_{\mathrm{wdc}i}}, \frac{R_{\mathrm{s}i}}{L_{\mathrm{s}i}}, \frac{R_{\mathrm{s}i}}{L_{\mathrm{s}i}}, \frac{1}{C_{\mathrm{dc}i}}\right]$$

and $\boldsymbol{\epsilon}_i$ is a positive constant which is an approximation error of uncertainty representation. The uncertainty matrix is calculated as the difference of the matrices $\boldsymbol{M}_i$ and $\boldsymbol{A}_i$. The matrix $\boldsymbol{A}_i$ is calculated at nominal operating points and $\boldsymbol{M}_i$ at arbitrary points to model the uncertainties. Prior to the controller design, several large disturbance simulations are carried out to get an idea of the region of interest. The maximum value of $\|\boldsymbol{M}_i - \boldsymbol{A}_i\|$ is obtained over this region and not globally. If the maximum value is evaluated over the entire uncertainty region, the calculation burden will be very high and it will lead to a conservative controller. The complete description of this reformulation technique can be found in [32] and [33]. The formulation presented above is used in the next section to design a distributed output-feedback controller that coordinates the active and reactive power productions of DG units and STATCOM/ESS devices.

III. PROPOSED CONTROL SCHEME

A single microgrid system, operated in islanded mode, shows several deficiencies, including low reliability and limited energy generation capability. This issue can be solved through the interconnection of multiple microgrids that respond to power unbalances by adjusting the powers flowing to and from the interconnected microgrid modules. The configuration considered in this paper consists of a STATCOM/ESS module to control both the active and reactive power of the microgrid. Inverters and ESSs are used to exchange power among interconnected microgrids through tie-lines. The power transfer among the interconnected microgrids is controlled based on frequency measures. An example of the proposed topology is shown in Fig. 5.

The proposed architecture of the distributed control is shown in Fig. 6. The distributed control layer is used for coordinating inverters and STATCOM/ESS devices whereas local droop controllers as discussed, for example, in [28], [34] are used
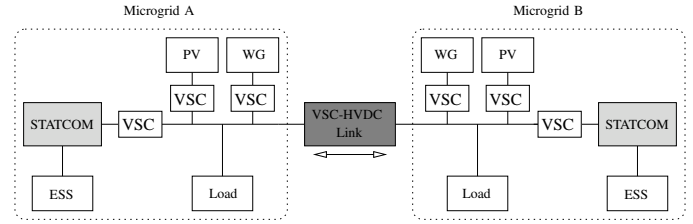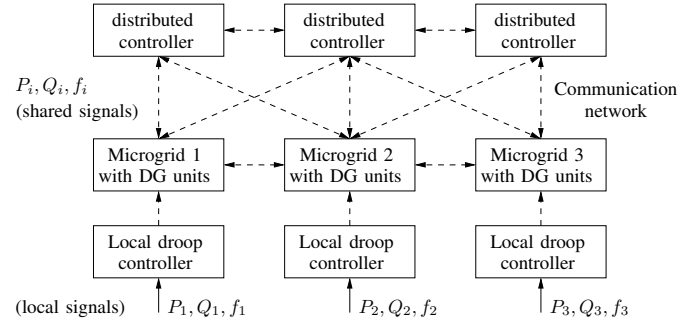

Fig. 5.   Interconnection between two microgrids.

Fig. 6.   Architecture of the distributed control scheme.

for the DG units. Each microgrid incldes several distributed energy resources which have their own local controllers. These controllers monitor real power, reactive power and frequency of that particular microgrid and share powers through VSC-HVDC link appropriately in order to ensure the stability of the overall system. Distributed controllers monitor real power mismatch between generation and load demand, reactive power mismatch between generation and load demand and frequency deviation of neighbouring microgrids using the communication network. If there is a mismatch between active or reactive power generation and demand in a microgrid, the controllers communicate to each others and regulate power flow through VSC-HVDC to meet the demand. Mismatches of active power ($\Delta P_i = P_{gi} - P_{di}$), reactive power ($\Delta Q_i = Q_{gi} - P_{di}$) and frequencies ($\Delta f_i = 50 \pm f_i$) are shared between microgrids and distributed controllers using the communication network as indicated in Fig. 6. These signals are chosen for the controllers by the method of comparing the residuals, which are the products of modal controllability and observability gramians [31]. The information among neighboring subsystems is exchanged using the communication network which is simpler and more reliable compared to the centralized control as in centralized control information is transmitted over a long distance. Digital communication networks allow the communication between the subsystems and thereby provide a larger flexibility for control design: instead of only local subsystem information also neighboring subsystems states can be used for the distributed control. As a result, a better performance is achieved compared to the decentralized approach. The controllers of the STATCOM/ESS and that of the inverter work as follows.

1) STATCOM/ESS controller: As it is shown in Fig. 4 of the previous section, this controller provides real power and frequency command to achieve the desired system response
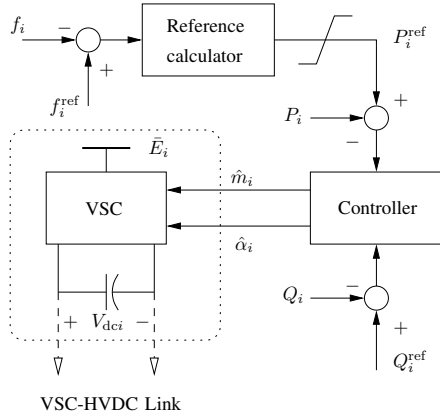
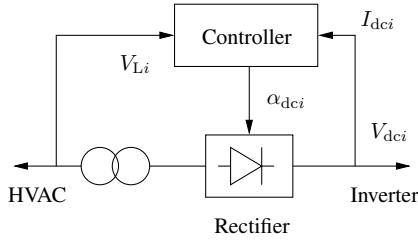Fig. 7. Structure of the proposed inverter control.

Fig. 8. Structure of the proposed rectifier control.

during the transient period. The proposed controller regulates the modulation gain (m_{1i}) and firing angle (α_{1i}). The firing angle, α_{1i} mainly affects the variation of the active power exchanged among different microgrid clusters. Therefore, the function of the active power control is to meet the active power demand of the system during transients. The other output of the controller is the duty cycle ratio, m_{1i} which mainly regulates the magnitude of the STATCOM's output voltage and therefore the system voltage.

2) Converter controller: The active power flow among the microgrids is controlled through the firing angle $\hat{\alpha}_i$ and the output DC voltage V_{dci} of VSC converter of the VSC-HVDC link between microgrids. The control chain is shown in Fig. 7. The frequency error ($f_i^{\mathrm{ref}} - f_i$) allows defining the power flows among microgrids in both transient and steady-state conditions. The reference active power P_i^{ref} is generated from the control scheme as shown in Fig. 7 using the frequency error ($f_i^{\mathrm{ref}} - f_i$) of a microgrid. The frequency of a microgrid deviates when there is mismatch between its generation and load demand. The reference calculator is a constant and its value is given as 0.25 MW/Hz. The input DC voltage of the inverter is controlled by a rectifier control circuit as shown in Fig. 8.

The proposed controllers for the STATCOM/ESS and the VSC-HVDC link are given as [35]:

$$\boldsymbol{u}_i = \boldsymbol{u}_{\mathrm{f}i} - \boldsymbol{u}_{\mathrm{ad}i} \qquad (14)$$

where

$$\boldsymbol{u}_{\mathrm{f}i} = \rho_i \boldsymbol{K}_i \hat{\boldsymbol{e}}_i \qquad (15)$$

$$\boldsymbol{u}_{\mathrm{ad}i} = \hat{\boldsymbol{W}}_i^T \boldsymbol{\varphi}_i(\hat{\boldsymbol{x}}_i) \qquad (16)$$

where ρ_i is a coupling strength gain which is chosen using trial and error method and $\varphi_i(\hat{\boldsymbol{x}}_i)$ is a known vector. $\boldsymbol{K}_i$ is a feedback matrix and given as:

$$\boldsymbol{K}_i = -\boldsymbol{B}_i^T \boldsymbol{G}_i \qquad (17)$$

where $\boldsymbol{G}_i$ is the unique positive definite solution to the following Riccati equation:

$$\boldsymbol{A}_i^T \boldsymbol{G}_i + \boldsymbol{G}_i \boldsymbol{A}_i + \boldsymbol{H}_i - \boldsymbol{G}_i \boldsymbol{B}_i \boldsymbol{B}_i^T \boldsymbol{G}_i = \boldsymbol{0} \qquad (18)$$

where $\boldsymbol{H}_i$ is a positive definite matrix. The vector $\hat{\boldsymbol{e}}_i$ is defined as

$$\hat{\boldsymbol{e}}_i = \sum_{j=0}^{N} a_{ij}(\hat{\boldsymbol{x}}_i - \hat{\boldsymbol{x}}_j) \qquad (19)$$

where a_{ij} is the element (i, j) of the adjacence matrix that defines the interconnections of the microgrids[1] and $\hat{\boldsymbol{x}}_i$ is an estimation of $\boldsymbol{x}_i$ obtained using a state observer described by:

$$\begin{aligned} \dot{\hat{\boldsymbol{x}}}_i &= \boldsymbol{A}_i \hat{\boldsymbol{x}}_i + \boldsymbol{B}_i \boldsymbol{u}_{\mathrm{f}i} + \boldsymbol{F}_i(\boldsymbol{y}_i - \hat{\boldsymbol{y}}_i) \\ \hat{\boldsymbol{y}}_i &= \boldsymbol{C}_i \hat{\boldsymbol{x}}_i \end{aligned} \qquad (20)$$

where $\boldsymbol{F}_i$ is an observer gain matrix designed such that $\boldsymbol{A}_{ei} = \boldsymbol{A}_i - \boldsymbol{F}_i \boldsymbol{C}_i$ is Hurwitz (stable).

The term $\boldsymbol{u}_{\mathrm{ad}i}$ is an adaptive term that compensates for the uncertainty term $\boldsymbol{\psi}_i(\boldsymbol{x}_i)$ and $\hat{\boldsymbol{W}}_i$ in (16) is an estimate of $\boldsymbol{W}_i$ defined by (13). The matrix $\hat{\boldsymbol{W}}_i$ that is obtained as

$$\dot{\hat{\boldsymbol{W}}}_i = \gamma_i \left[\boldsymbol{\varphi}_i(\hat{\boldsymbol{x}}_i)\tilde{\boldsymbol{y}}_i^T - \frac{1}{2\kappa_i}\boldsymbol{\varphi}_i(\hat{\boldsymbol{x}}_i)\boldsymbol{\varphi}_i^T(\hat{\boldsymbol{x}}_i)\hat{\boldsymbol{W}}_i - r_i\hat{\boldsymbol{W}}_i \right] \quad (21)$$

where $\tilde{\boldsymbol{y}}_i = \boldsymbol{y}_i - \hat{\boldsymbol{y}}_i$, and κ_i, γ_i and r_i are positive constants which are chosen using a successive approximation technique. In this paper, $\epsilon_i = 0.25$, $\rho_i = 8.25$, $\gamma_i = 150$, $\kappa_i = 0.05$ and $r_i = 0.60$, which provide feasible controllers.

The closed loop system is uniformly ultimately bounded if the coupling strength gain ρ_i satisfies

$$\rho_i \geq \frac{1}{2\min \tau_i(\boldsymbol{H}_i)} \qquad (22)$$

where τ_i are the eigenvalues of $\boldsymbol{H}_i$. The control algorithm for DG units using the above control scheme is shown in Fig. 9.

IV. CASE STUDY

The test system considered in this paper is shown in Fig. 10. It is composed of three interconnected microgrids. Each microgrid consists of a PV unit, a fully controlled wind generator (WG), a STATCOM/ESS and mixture of static and dynamic loads. The capacity of the STATCOM is 0.5 MVA and ESS is 0.6 MWh. In the paper, the length of the DC lines of the VSC-HVDC links is assumed to be about 50 km. The PV unit and wind turbine in microgrids 1 and 2 work at rated conditions as depicted in Fig. 10. Under normal operating conditions when three microgrid are interconnected, 0.8 MW is delivered from

---

[1]The adjacence matrix is built as follows: $a_{ij} = 1$ if the macrogrid i is connected to the microgrid j; $a_{ij} = 0$ otherwise.
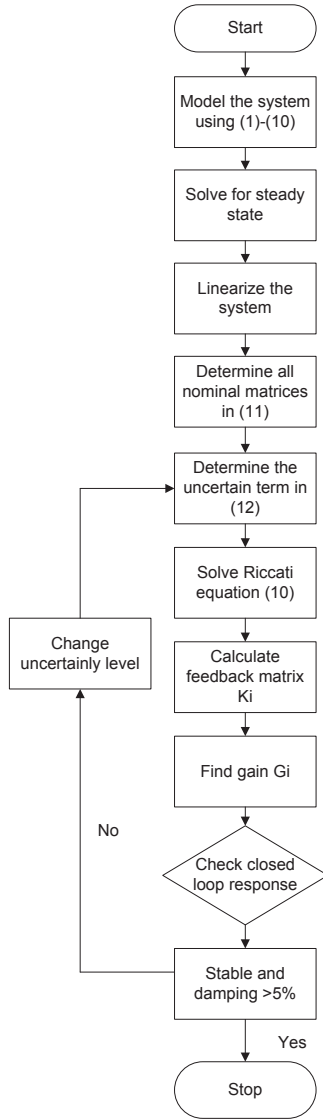
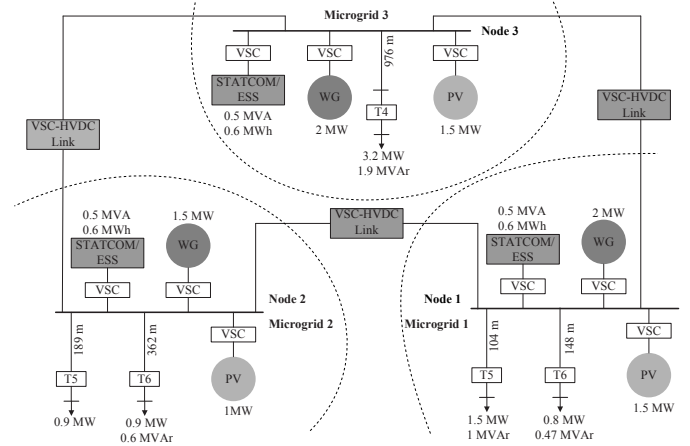Fig. 9. Flowchart of the proposed control algorithm

Fig. 10. Single line diagram of the test system.

case study presents and discusses the following points: (i) the interaction of conventional non-communicating local DG controllers; (ii) a comparison of the performance of distributed and decentralized controllers; (iii) the response of the designed controller after the outage of a communication link; (iv) the response of the proposed controller after the disconnection of a DG unit; (v) the designed of the proposed controller due to parameter uncertainties; and (vi) the response of the designed controller with dynamic and severe unbalanced load.

A. Interaction of non-communicating local DG controllers

This subsection discusses the behavior of conventional local DG controllers in a system where several microgrids are connected together. It has been assumed that no communication among the microgrids. The analysis is carried out using the STATCOM/ESS and VSC-HVDC link models as shown in Fig. 4 and Figs. 7 and 8, respectively, and using a second-order PI controller as presented in [3]. PI parameters are generally tuned by trial-and-error approaches. The initial guess can be obtained, for example, using the Ziegler-Nichols method [37]. We adopt this strategy to define the optimal settling time and peak overshoot. In this case, the gains of the tuned (trial-and-error method) PI controller for STATCOM/ESS are K_p=5 and K_I=40. Each DG unit with a PI controller defines a 9th-order system whereas the STATCOM/ESS module with a PI controller is a fifth-order system. The total states in per each microgrid with two DG units and one STATCOM/ESS are 31. The whole system with three microgrids has thus 93 state variables.

Figure 11 shows the eigenvalues of the dominant modes for three scenarios: (i) microgrid 3 alone, (ii) microgrids 1 and 3, and (iii) microgrids 1, 2 and 3. Connecting together the microgrids significantly reduces the damping as the eigenvalues move towards the imaginary axis. Observe also that the right-most eigenvalues have a damping ratio lower than 5%. The main conclusion is that dominant modes of neighboring microgrids are coupled and their interaction tends to destabilize the overall system.
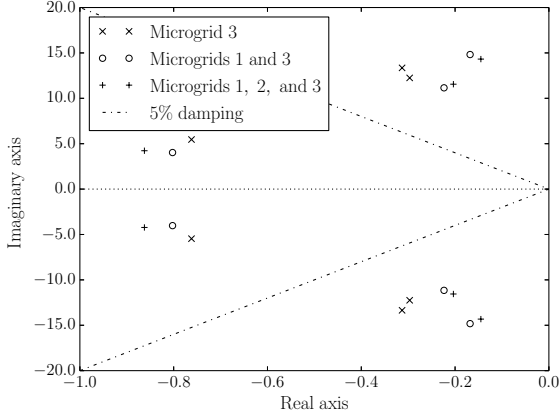
microgrid 1 to microgrid 3, 0.4 MW from microgrid 2 to 3, whereas microgrids 1 and 2 do not exchange power. We assume that, if only two microgrids (1 and 2) are interconnected, they do not share any power in steady-state. A preliminary analysis is carried out using conventional controllers, which are designed without sharing any information with each other [3]. Then the designed control scheme is studied. To compare the behavior of conventional and proposed control schemes, both a small-signal analysis and time-domain simulations following a large disturbance are carried out. The objective of this case study is to illustrate the interactions of multiple microgrids and investigate the performance of the designed controller under various operating conditions of the test system. The proposed controller is implemented in Matlab/Simulink, which is used to solve all simulations presented in this section. The

Fig. 11. Dominant modes of a single microgrid as well as of multiple interconnected microgrids.

Fig. 13. Eigenvalues of the system composed of three microgrids using decentralized [38] and distributed controllers.
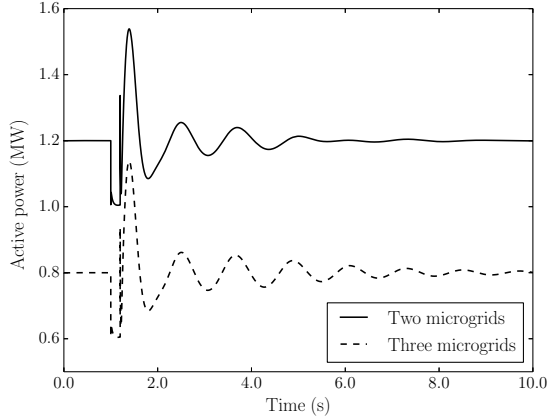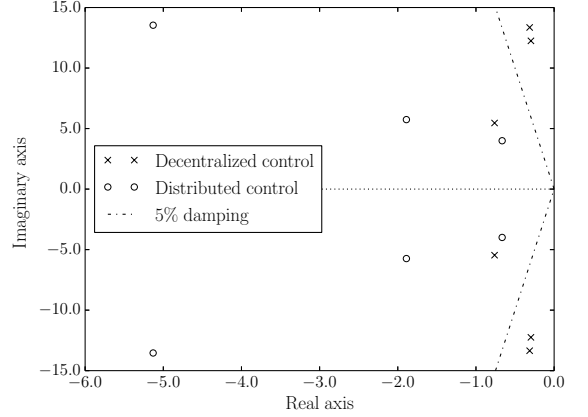

Fig. 12. Active power flow from microgrid 1 to microgrid 3 for three-phase fault at node 3.

Time-domain simulations are carried out to observe the behavior of the interconnected microgrids following a large disturbance. In particular, a three-phase fault is applied at node 3 of microgrid 3 at $t = 1$ s. The fault is cleared after 100 ms. Figure 12 shows the power flow from microgrid 1 to microgrid 3 when only two microgrids (i.e., 1 and 3) and three microgrids (i.e., 1, 2 and 3) are in operation. Simulation results confirm that the inclusion of a third microgrid reduces the system damping, thus having a negative impact on the overall dynamic performance of the system. A comparison of the performances between the designed controller and decentralized controller are shown in Table I.

TABLE I. PERFORMANCE COMPARISON: (a) PROPOSED CONTROLLER; AND (b) DECENTRALIZED CONTROL

(a) Proposed Controller			(b) Decentralized Control		
damping	overshoot	settling time	damping	overshoot	settling time
16.5%	12.5%	1.25 s	2.42%	87.5%	7.25 s

B. Comparison of decentralized control without communication and the designed distributed control

This subsection compares the performance of the designed controller with a fully decentralized controller that does not share information among microgrids as proposed in [38]. Both small-signal and large disturbance analyses are considered. The most critical eigenvalues with the fully decentralized controller as well as of the designed distributed controller are shown in Fig. 13. As it can be observed, the decentralized control shows poorly damped eigenvalues, i.e., eigenvalues with a damping ratio lower than 5%. On the other hand, the distributed controller leads to a properly damped system.

A time-domain simulation considering the complete nonlinear system and a three-phase fault is carried out to determine the performance of the proposed controller. The three-phase fault is applied at node 3 of microgrid 3 at $t = 1$ s and subsequently cleared after 100 ms.

Figure 14 shows the power flow from microgrid 2 to microgrid 3, when all microgrids (1, 2 and 3) are connected and in operation. From Fig. 14, it appears that the designed distributed controller is robust and provides an excellent performance in terms of overshoot, rise time, settling time, oscillation and steady-state errors. The designed controller provides better performance irrespective of the number of microgrids, i.e., one, two or three.

C. Failure of a communication link

Firstly, it is assumed that the communication link between microgrids 1 and 2 fails. A three-phase fault is applied at node 3 in microgrid 3 at $t = 1$ s. The fault is cleared by the auto-reclosing action of the circuit breaker after 100 ms. Figures 15 and 16 show the active power output and terminal voltage, respectively, for the WG in microgrid 2. Then, the effect of the communication link failure between two other microgrids (i.e., 1 and 3) is investigated to study the worst-case scenario. An asymmetrical fault (single line to ground) is applied at the interconnecting line of microgrids 1 and 2 at 0.03 s which
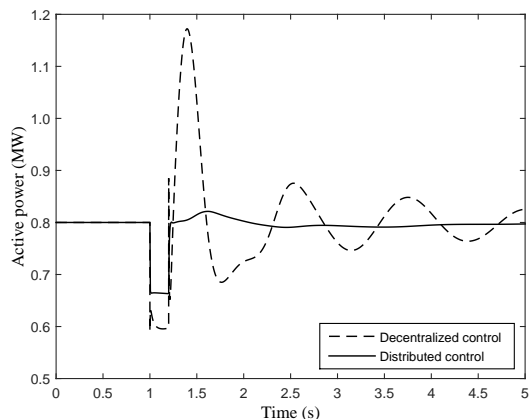
Fig. 14.   Active power flow from microgrid 1 to microgrid 3 for three-phase fault at node 3 with distributed and decentralized controllers.
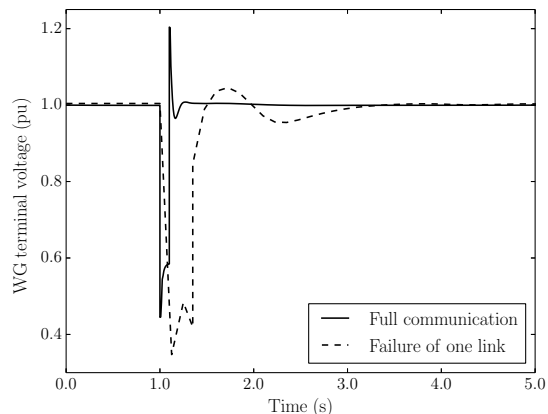

Fig. 16.   Terminal voltage of wind generator in microgrid 2 for three-phase fault at node 3 with and without full communication.
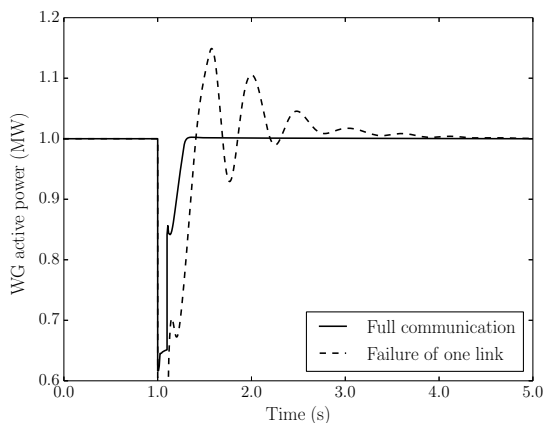

Fig. 15.   Active power of wind generator in microgrid 2 for three-phase fault at node 3 with and without full communication.
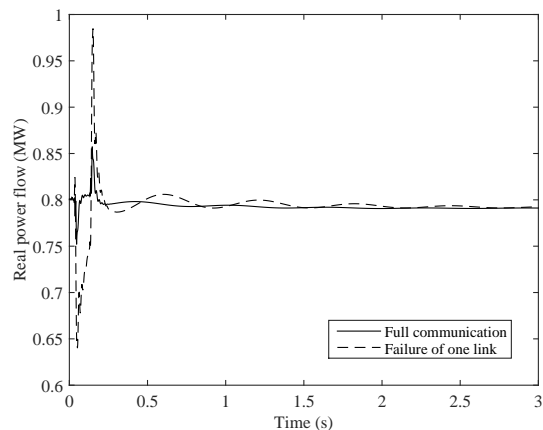

Fig. 17.   Power flow from microgrid 1 to microgrid 3 for asymmetrical fault with and without full communication.

is cleared at 0.13 s. Figure 17 shows the power flow from microgrid 1 to 3. The designed controller with full communication ensures stable operation during severe transients and provides desired dynamic performance during the post-fault condition. The quantitative comparison of the performance of the distributed controller with full communication and partial communication (like decentralized control) is shown in Table II. Each DG controller autonomously and effectively responds to the disturbance and stabilizes the system within one second. In case one communication link fails, simulation results indicates that the proposed controller is still able to recover a stable operating condition after the clearance of the fault. However, the lack of one communication channel affects the overall performance of the controller. The main conclusion that can be drawn from this case study is that the reliability of the communication network is crucial for the correct operation of multiple interconnected microgrids.

D. Outage of a DG unit

In this case study, the outage of a PV unit in microgrid 3 is considered at $t=1$ s. To counteract the consequence of power unbalance, the controller responds by increasing both active and reactive power supply based on the availability in the three microgrids. In particular, the STATCOM/ESS and interconnecting VSC-HVDC Link provide extra active power, 0.5 and 1 MW, respectively, to balance the load demand. DG units continue to operate at their assigned set point. Figure 18 shows the power flow from microgrid 1 to microgrid 3; and Fig. ?? shows the reactive power output of the STATCOM/ESS

TABLE II.   PERFORMANCE COMPARISON: (a) PROPOSED CONTROLLER (FULL COMMUNICATION); AND (b) PARTIAL COMMUNICATION

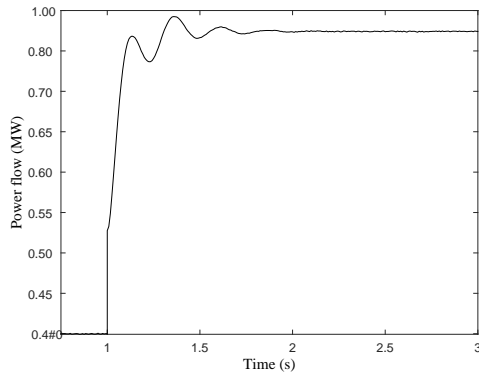| (a) Full communication			(b) One link fail		
damping	overshoot	settling time	damping	overshoot	settling time
16.5%	5.0%	0.20 s	5.25%	15%	4.2 s

Fig. 18. Active power flow from microgrid 2 to microgrid 3 for outage of DG unit.

TABLE III. PERFORMANCE COMPARISON: (a) PROPOSED CONTROLLER; AND (b) DECENTRALIZED CONTROLLER

(a) Distributed controller			(b) Decentralized controller		
damping	overshoot	settling time	damping	overshoot	settling time
16.5%	1.5%	2.2 s	5.25%	27.5%	4.1 s

in microgrid 3. Simulation results indicate that the proposed control scheme makes the microgrids to cooperate and share the power flow to stabilize the system. Moreover, the designed controller provides an excellent performance in terms of damping ratio and settling time. The quantitative comparison of the performance of the designed distributed controller and decentralized control is shown in Table III.

E. Effect of parameter uncertainties

Uncertainties in power systems can be caused by the variation of loading, load parameters, network topology and machine parameters. It is difficult to identify the parameters of power systems in particular the exact load demand as it changes continuously. The designed controller in this paper provides robust performance against parameter uncertainties.

Although the controller is designed for rated operating conditions, it is robust, i.e., parameter uncertainties do not affect its dynamic performance. The performance of the controller is tested under a severe load change (20%) and compared with a decentralized controller and without controller as shown in Fig. 19. Without control, the system is unstable. Moreover, although both distributed and decentralized controls stabilize the system, the speed drops only by 2% when using the proposed distributed controller and more than 6% when considering a decentralized controller.

Figure 20 shows the load voltage at microgrid 3 with accurate line parameters and modified line parameters (20%). A three-phase short-circuit fault is applied at $t=1$ s and cleared after five cycles. Figure 20 shows that the proposed distributed controller is robust against parameter variations.
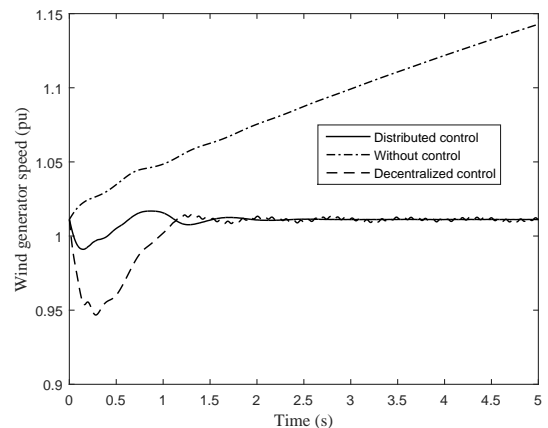

Fig. 19. Speed of wind generator in microgrid 3 for sudden severe change in connected load.
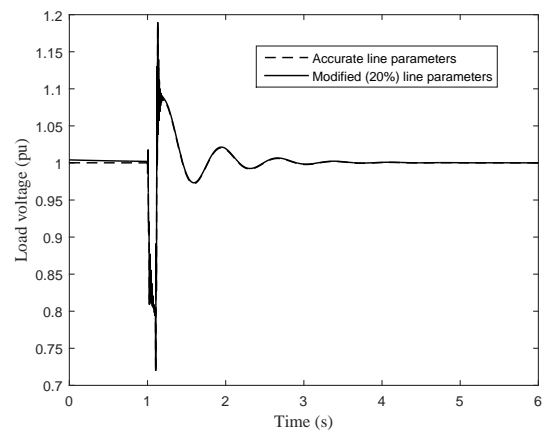

Fig. 20. Load voltage with accurate and modified (20%) line parameters.

F. Effect of dynamic load and unbalanced load

In this subsection, we assume that a significant portion of the connected load (60%-70%) of each microgrid is composed of induction motors (IMs). The purpose of this section is to test the impact on the performance of the proposed control scheme if the system include a large amount of dynamic nonlinear loads under unbalanced conditions. Figure 21 shows the terminal voltage of the wind generator of microgird 1 due to its unbalanced loading conditions as shown in Figures 22. Results shows that the designed controller is robust and properly respond to unbalanced conditions. Moreover, the presence of dynamic loads such as IMs does not compromise the performance of the controller.

V. CONCLUSIONS

A systematic procedure to design distributed controllers to regulate the power flow among multiple islanded microgrids is proposed in this paper. It is shown that conventional local control schemes are unable to provide a satisfactory dynamic
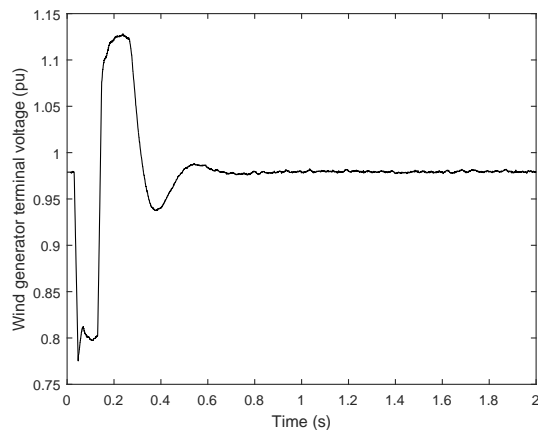
Fig. 21. Terminal voltage of wind turbine at microgrid 1 for unbalanced load.
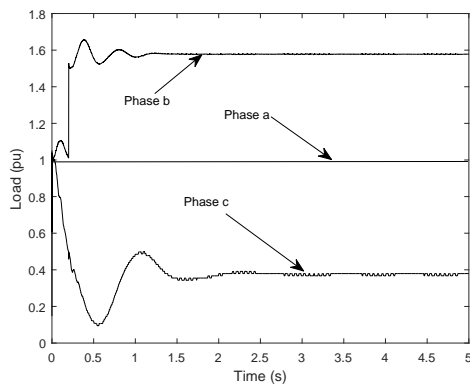

Fig. 22. Unbalanced load.

response if the microgrids are interconnected. A key aspect is that microgrids have to exchange information. However, a fully centralized control approach is unfeasible and, likely, not economically viable. The proposed controller relies on a distributed output feedback-tracking control strategy that, while based on a communication network, is simpler and cheaper to implement than a centralized controller.

Based on simulation results, the proposed control appears robust and responds properly to parameter uncertainty as well as large disturbances. However, since the proposed control scheme relies on a communication network, the failure of some communication channel can sensibly reduce the dynamic repones of the system.

Future work will focus on the design of a distributed controller considering more complex microgrids topologies and nonlinear loads. Along with this, the approach to reduce the effect of failures and/or delays of the communication network will also be investigated.

REFERENCES

[1] J. A. Pecas Lopes, N. Hatziargyriou, J. Mutale, P. Djapic and N. Jenkins, "Integrating distributed generation into electric power systems: A review of drivers, challenges and opportunities," *Electric Power Systems Research*, vol. 77, no. 9, pp. 1189-1203, July 2007.

[2] K. Buayai, W. Ongsakul and N. Mithulananthan, "Multi-objective micro-grid planning by NSGA-II in primary distribution system," *Euro. Trans. on Elec. Power*, vol. 22, no. 2, pp. 170-187, Mar. 2012.

[3] Y. Hida, K. Koyanagi, R. Yokoyam, S. Nagata, K. Nakao and T. Hirai, "Electricity cluster-oriented network: a grid-independent and autonomous aggregation of microgrids," *Proc. of the International Symposium on Modern Electric Power Systems*, 20-22 Sept. 2010, Wroclaw, pp. 1–6.

[4] R. H. Lasseter, "Smart distribution: coupled microgrids," *Proceedings of the IEEE*, vol. 99, no. 6, pp. 1074–1082, June 2011.

[5] H. S. V. S. Kumar Nunna and S. Doolla, "Demand response in smart distribution system with multiple microgrids," *IEEE Trans. on Smart Grid*, vol. 3, no. 4, pp. 1641–1649, Dec. 2012.

[6] A. L. Dimeas and N. D. Hatziargyriou, "Agent based control for microgrids," *IEEE PES Gene. Meeting*, June 2007, Tampa, pp. 1-5.

[7] C. M. Colson and M. H. Nehrir, "Comprehensive real-time microgrid power management and control with distributed agents," *IEEE Trans. on Smart Grid*, vol. 4, no. 1, pp. 617–627, Mar. 2013.

[8] A. Bidram, A. Davoudi, F. L. Lewis and J. M. Guerrero, "Distributed cooperative secondary control of microgrids using feedback linearization," *IEEE Trans. on Power Systems*, vol. 28, no. 3, pp. 3462–3470, Aug. 2013.

[9] A. Maknouninejad, Z. Qu, J. Enslin and N. Kutkut, "Clustering and cooperative control of distributed generators for maintaining microgrid unified voltage profile and complex power control," *IEEE PES Transmission and Distribution Conference and Exposition*, 7-10 May 2012, Orlando, pp. 1–8.

[10] G. Díaz, C. González-Morán, J. Gómez-Aleixandre and A. Diez, "Complex-valued state matrices for simple representation of large autonomous microgrids supplied by PQ and Vf generation," IEEE Trans. on Power Systems, vol. 24, no. 4, pp. 1720–1730, Nov. 2009.

[11] J. M. Guerrero, J. C. Vasquez, J. Matas, L. G. de Vicua and M. Castilla, "Hierarchical control of droop-controlled AC and DC microgrids: A general approach toward standardization," *IEEE Trans. on Industrial Electronics*, vol. 58, no. 1, pp. 158–172, Jan. 2011.

[12] A. G. Tsikalakis and N. D. Hatziargyriou, "Centralized control for optimizing microgrids operation," *IEEE Trans. on Energy Conversion*, vol. 23, no. 1, pp. 241–248, Mar. 2008.

[13] H. Liang, B. J. Choi, W. Zhuang and X. Shen, "Stability enhancement of decentralized inverter control through wireless communications in microgrids," *IEEE Trans. on Smart Grid*, vol. 4, no. 1, pp. 321–331, Mar. 2013.

[14] P. H. Divshali, A. Alimardani, S. H. Hosseinian and M. Abedi, "Decentralized cooperative control strategy of microsources for stabilizing autonomous VSC-based microgrids," *IEEE Trans. on Power Systems*, vol. 27, no. 4, pp. 1949–1959, Nov. 2012.

[15] C. Ahn and H. Peng, "Decentralized voltage control to minimize distribution power loss of microgrids," *IEEE Trans. on Smart Grid*, vol. 4, no. 3, pp. 1297–1304, Sep. 2013.

[16] P1. Y. Mohamed and E. F. El-Saadany, "Adaptive decentralized droop controller to preserve power sharing stability of paralleled inverters in distributed generation microgrids," *IEEE Trans. on Power Electronics*, vol. 23, no. 6, pp. 2806–2816, Nov. 2008.

[17] J. M. Guerrero, L. G. De-Vicuna, J. Matas, M. Castilla and J. Miret, "A wireless controller to enhance dynamic performance of parallel inverters in distributed generation systems," *IEEE Trans. on Power Electronics*, vol. 19, no. 5, pp. 1205–1213, Sep. 2004.

[18] P. Massioni and M. Verhaegen, "Distributed control for identical dynamically coupled systems: A decomposition approach, *IEEE Trans. on Automatic Control*, vol. 54, no. 1, pp. 124–135, Jan. 2009.

[19] H. Xin, Z. Qu, J. Seuss, A. Maknouninejad, "A self-organizing strategy for power flow control of photovoltaic generators in a distribution

network," *IEEE Trans. on Power Systems*, vol. 26, no. 3, pp. 1462–1473, Aug. 2011.

[20] S. Anand, B. G. Fernandes and M. Guerrero, "Distributed control to ensure proportional load sharing and improve voltage regulation in low-voltage DC microgrids," *IEEE Trans. on Power Electronics*, vol. 28, no. 4, pp. 1900–1913, Apr. 2013.

[21] M. Moradzadeh, R. Boel and L. Vandevelde, "Voltage coordination in multi-area power systems via distributed model predictive control," *IEEE Trans. on Power Systems*, vol. 28, no. 1, pp. 513–521, Feb. 2013.

[22] L. D. Marinovici, J. Lian, K. Kalsi, P. Du and M. Elizondo, "Distributed hierarchical control architecture for transient dynamics improvement in power systems," *IEEE Trans. on Power Systems*, vol. 28, no. 3, pp. 3065–3074, Aug. 2013.

[23] G. Turner, J. P. Kelley, C. L. Storm, D. A. Wetz and Wei-Jen Lee, "Design and active control of a microgrid testbed," IEEE Trans. on Smart Grid, vol. 6, no. 1, pp. 73–81, Jan. 2015.

[24] C. M. Colson and M. H. Nehrir, "Comprehensive real-time microgrid power management and control with distributed agents," IEEE Trans. on Smart Grid, vol. 4, no. 1, pp. 617–627, March 2013

[25] M. Fathi and H. Bevrani, "Statistical cooperative power dispatching in interconnected microgrids," *IEEE Trans. on Sustainable Energy*, vol. 4, no. 3, pp. 586–593, July 2013.

[26] M. J. Hossain, M. A. Mahmud, H. R. Pota, N. Mithulananthan and R. C. Bansal,"Distributed control scheme to regulate power flow and minimize interactions in multiple microgrids," IEEE PES General Meeting Conference & Exposition, 27-31 July 2014, pp.1–5.

[27] A. Ouammi, H. Dagdougui, L. Dessaint and R. Sacile, "Coordinated model predictive-based power flows control in a cooperative network of smart microgrids," IEEE Trans. on Smart Grid, no. 99, doi: 10.1109/TSG.2015.2396294, 2015.

[28] Y. A.-R. I. Mohammad and A. A. Radwan, "Hierarchical control system for robust microgrid operation and seamless mode transfer in active distribution systems, *IEEE Trans. on Smart Grid*, vol. 2, no. 2, pp. 352–362, June 2011.

[29] M. J. Hossain, H. R. Pota, M. A. Mahmud and M. Aldeen, "Robust control for power sharing in microgrids with low-inertia wind and PV generators," *IEEE Trans. on Sustainable Energy*, doi: 10.1109/TSTE.2014.2317801, May 2014.

[30] H. Shariatpanah and R. Fadaeinedjad and M. Rashidinejad, "A new model for PMSG-based wind turbine with yaw control, *IEEE Trans. on Energy Conversion*, vol. 28, no. 4, pp. 929–937, Dec. 2013.

[31] M. J. Hossain, H. R. Pota, V. Ugrinovskii and R. A. Ramos, "Simultaneous STATCOM and pitch angle control for improved fault ride-through capability of fixed-speed wind turbines," *IEEE Trans. on Sustainable Energy*, vol. 1, no. 3, pp. 142–151, Oct. 2010.

[32] M. J. Hossain, H. R. Pota, V. Ugrinovski and R. A. Ramos, "Voltage mode stabilisation in power systems with dynamic loads," *International Journal of Electrical Power and Energy Systems*, vol. 32, no. 8, pp. 911–920, November 2010.

[33] M. J. Hossain, T. K. Saha, N. Mithulananthan and H. R. Pota, "Control strategies for augmenting LVRT capability of DFIGs in interconnected power systems," *IEEE Trans. on Industrial Electronics*, vol. 60, no. 6, pp. 2510–2522, June 2013.

[34] J. M. Guerrero, L. García de Vicuna, J. Matas, M. Castilla and J.Miret, "A wireless controller to enhance dynamic performance of parallel inverters in distributed generation systems," *IEEE Trans. on Power Electronics*, vol. 19, no. 5, pp. 1205–1213, Sept. 2004.

[35] Z. Peng, D. Wang and H. Zhang, "Distributed output feedback tracking control of uncertain nonlinear multi-agent systems with unknown input of leader," *Advances in Neural Networks*, vol. 7952, pp. 11–18, July 2013.

[36] G. Ramtharan, A. Arulampalam, J. B. Ekanayake, F. M. Hughes, N.Jenkins, "Fault ride through of fully rated converter wind turbines with AC and DC transmission," IET Renewable Power Generation, vol. 3, no. 4, pp. 426–438, Dec. 2009.

[37] G. Mallesham, S. Mishra, and A. N. Jha, "Maiden application of ZieglerNichols method to AGC of distributed generation system, in Proc. *IEEE/PES Power Syst. Conf. Expo.*, Seattle, WA, Mar. 1518, 2009, pp. 17.

[38] A. H. Etemadi, E. J. Davison and R. Iravani, "A decentralized robust control strategy for multi-DER microgridsPart I: Fundamental concepts," *IEEE Trans. on Power Delivery*, vol. 27, no. 4, pp. 1843–1853, Oct. 2012.

Dr. Jahangir Hossain (M'10, SM'12) received B.Sc. and M.Sc. Eng. degrees from Rajshahi University of Engineering and Technology (RUET), Bangladesh, in 2001 and 2005, respectively, and a Ph.D. degree from the University of New South Wales, Australia, all in electrical and electronic engineering. He is currently working as lecturer in the discipline of Electrical and Electronic Engineering under the Griffith School of Engineering. Before joining at Griffith University, he served as a research fellow in the School of Information Technology and Electrical Engineering, University of Queensland, Australia. His research interests are renewable Energy integration and FACTS Devices with Energy Storage, smart grid, microgrids and distributed generations, dynamics, stability analysis and control, power electronics, electrical drives and intelligent control.

Dr. M. A. Mahmud (S'10, M'13) received the Bachelor degree in electrical and electronic engineering from Rajshahi University of Engineering and Technology (RUET), Bangladesh, in 2008 and the Ph.D. degree in electrical engineering from the University of New South Wales, Australia, with best thesis award in 2012. He worked as a research fellow at the University of Melbourne, Australia, and he is currently working as a lecturer at Deakin University, Australia. His research interests are dynamic stability of power systems, renewable energy integration, smart grids, nonlinear control theory, and electrical machine.

Dr. Federico Milano (SM'09) received from the University of Genoa, Italy, the Electrical Engineering degree and the Ph.D. degree in 1999 and 2003, respectively. From 2001 to 2002 he was a Visiting Scholar at the University of Waterloo, Canada. From 2003 to 2013, he was with the University of Castilla-La Mancha, Spain. In 2013, he joined the University College Dublin, Ireland, where he is currently Associate Professor. His research interests include power system modelling, stability and control.

Dr. Seddik Bacha (M'07) received the Engineering and Magister degrees form the Ecole National Polytechnique of Algiers (ENPA) in 1982 and 1990, respectively. He has been working as assistant professor at ENPA and Bgayet University until 1990. He joined the Grenoble Electrical Engineering Laboratory (G2Elab) and received the PhD and HDR degrees in 1993 and 1998, respectively. He is currently scientific advisor at the SuperGrid Institute of Energy Transition (France) and professor at the Joseph Fourier University of Grenoble, France. His main fields of interest are renewables integration, microgrids and HVDC Transmission grids.

Dr. Ahmad Hably was born in Saida, Lebanon. He received the B.S. degree in electrical engineering from the Lebanese University, Beirut, and the Ph.D. de- gree in automatic control from the Grenoble Institute of Technology (Grenoble INP), Grenoble, France, in 2007. After one year as Researcher at the Laboratoire dInformatique, de Robotique et de Microlectron- ique de Montpellier, he joined the Au- tomatique Control Department, GIPSA-Laboratory, Grenoble, as an Associate Professor.